Research Article | Vol. 26, No. 15 | 23 Jul 2018 | OPTICS EXPRESS 19235
Optics EXPRESS

Discrete temporal Talbot effect in synthetic mesh lattices

SHULIN WANG,[1] CHENGZHI QIN,[1] BING WANG,[1,*] AND PEIXIANG LU[1,2,3]

[1]*School of Physics and Wuhan National Laboratory for Optoelectronics, Huazhong University of Science and Technology, Wuhan, 430074, China*
[2]*Laboratory for Optical Information Technology, Wuhan Institute of Technology, Wuhan, 430205, China*
[3]*lupeixiang@hust.edu.cn*
**wangbing@hust.edu.cn*

Abstract: We investigate the discrete temporal Talbot effect in a synthetic mesh lattice by employing two coupled fiber loops with different lengths. The lattice consists of the round-trip number and time delay of pulse trains propagating in the fiber loops. The Talbot effect occurs only as the incident pulse train in one loop has a temporal period that is 1, 2, or 4 folds of time interval corresponding to the length difference of the two loops. By varying the splitting ratio of coupler connecting the two loops, the lattice band structure can be engineered and so do the Talbot distance, which can be further tuned by imposing an initial linear phase distribution on the incident pulse train. In addition, the incident periods for Talbot effect can also be fractional fold by using time multiplexing. The study may find applications in temporal cloaking, passive amplifying, and pulse repetition rate multiplication.

1. Introduction

Talbot effect refers to self-imaging phenomena as the periodic structure is illuminated by a coherent light beam, which was firstly reported by H. F. Talbot in 1836 [1]. The effect was later explained by the Fresnel diffraction theory [2]. The Talbot image usually locates at multiple Talbot distance. Moreover, the fractional Talbot images with squeezed period also exist at rational multiples of Talbot distance [3–5]. Due to the analogy between spatial Fresnel diffraction and second-order temporal dispersion, the Talbot effect can be extended to time domain aiming to realize recurrence of periodic pulse trains [6,7]. The fractional Talbot effect also exists in time domain, which could increase the repetition rate of pulse trains [8–11]. The temporal Talbot effect has found wide applications in high-speed signal generation, passive amplification, and temporal cloaking for the purpose of optical communication and signal processing [8–16].

On the other hand, the Talbot effect can be realized in discrete optical systems such as waveguide arrays [18–25]. Unlike the Talbot effect in continuous medium, which is independent of the incident period, the discrete Talbot effect occurs only as the incident field has specific set of periodicities [18]. The discrete system has already been generalized from real space to other synthetic dimensions. For example, the temporal and spectral lattices were proposed to simulate diffraction effects, that is, the evolution of temporal pulse and light spectrum during propagation [26–31]. Recently, the synthetic temporal mesh lattice based on two coupled fiber loops with slightly different length has been proposed to realize large-scale PT-symmetry networks and the measurements of topological invariants [27,30].

In this work, we shall investigate the discrete temporal Talbot effect in the synthetic mesh lattice constructed by two coupled fiber loops. The lattice is two-dimensional and is formed by the round-trip number and time delay of pulse trains propagating in the fiber loops. The Talbot effect occurs only if the incident period is chosen as certain specific values, which are different from that in waveguide arrays due to the two dimension in periodicity. By changing the splitting ratio of the coupler that connects the two fiber loops, the band structure of synthetic mesh lattice can be engineered, resulting in the variation of Talbot distance.

#331367 https://doi.org/10.1364/OE.26.019235
Journal © 2018 Received 10 May 2018; revised 10 Jul 2018; accepted 11 Jul 2018; published 16 Jul 2018

Optics EXPRESS

Additionally, the Talbot distance is also tunable by modulating the distribution of initial phases imposed on the incident pulse trains. The Talbot effect can also be observed even if the incident period of pulse train becomes fractional fold of the lattice period. The unique features in the temporal mesh lattice are hard to obtain in the spatial counterparts.

2. Theory

We start by considering the synthetic mesh lattice constructed by the coupled fiber-loop circuit. As shown in Fig. 1(a), the circuit consists of two fiber loops connected by a 50:50 directional coupler. The length difference between two loops is ΔL which corresponds to a time delay of $2\Delta T = \Delta L/c_F$, where c_F is the light speed in the fiber. Here we inject a periodic pulse train to the long loop. After the initial pulse sequence passes through the coupler, two new pulse trains are generated and flow into two loops. A round trip later, the pulse sequence in long loop experiences a time delay $2\Delta T$ compared to the one in short loop. The interference between two pulse trains occurs as they meet at the coupler. The pulse trains will evolve in a stepwise manner with the increase of round-trip number, as shown in the bottom insert in Fig. 1(b). Considering that the evolution of the pulse trains is similar to the beam dynamics in the spatial mesh lattice, the equivalent mesh lattice for the two coupled fiber loops is established, as shown in Fig. 1(b). The axis m corresponds to the times the pulse trains enters the coupler connecting two fiber loops, and n is the relative position of pulse in the train. The evolution of amplitudes can be described by

$$\begin{aligned} u_n^m &= \frac{1}{\sqrt{2}}\left(u_{n+1}^{m-1} + iv_{n+1}^{m-1}\right), \\ v_n^m &= \frac{1}{\sqrt{2}}\left(iu_{n-1}^{m-1} + v_{n-1}^{m-1}\right), \end{aligned} \tag{1}$$

where *um n* and *vm n* denote the complex amplitudes of pulses in short and long loops, respectively [26,27]. The Bloch modes in this lattice can be written as

$$\begin{pmatrix} u_n^m \\ v_n^m \end{pmatrix} = \begin{pmatrix} U_0 \\ V_0 \end{pmatrix} e^{iQn/2} e^{i\theta m/2}, \tag{2}$$

in which $(U_0, V_0)^T$ is the eigen vector, Q and θ are the transverse Bloch momentum and longitudinal propagation constant of Bloch mode, respectively [26,27]. Substituting Eq. (2) into Eq. (1), we can obtain the band structure

$$\cos\theta = \frac{1}{2}(\cos Q - 1). \tag{3}$$

As illustrated in Fig. 1(c), two bands are symmetric in both θ and Q.

Considering the discreteness in the transverse direction, the input field distribution has a period of N in the synthetic mesh lattice [Fig. 1(b)], where N is a positive integer. Accordingly, the period of the initial pulse train is $N\Delta T$, as shown in Fig. 1(a). To satisfy the periodic boundary condition, the Bloch momentum Q is in the form of

$$Q_l = 2\pi l / \mathcal{N}, \tag{4}$$

in which $\mathcal{N} = N/2$, and $l = 0, 1 \ldots \mathcal{N} - 1$ [18,21]. The corresponding propagation constant at jth band is

$$\theta_{j,l} = \begin{cases} -\arccos[(\cos Q_l - 1)/2] & (j = 1), \\ \arccos[(\cos Q_l - 1)/2] & (j = 2), \end{cases} \tag{5}$$

Optics EXPRESS

where j is the band index. The pulse dynamics is a superposition of Bloch modes

$$\begin{pmatrix} u_n^m \\ v_n^m \end{pmatrix} = \sum_{j=1}^{2} \sum_{l=0}^{\mathcal{N}-1} c_{j,l} \begin{pmatrix} U_{j,l} \\ V_{j,l} \end{pmatrix} \exp(iQ_l n/2) \exp(i\theta_{j,l} m/2), \tag{6}$$

where $(U_{j,l}\ V_{j,l})^{\mathrm{T}}$ and $c_{j,l}$ are the eigen vector and coefficient, respectively. To realize the Talbot self-imaging, all modes contained should be able to exhibit recurrence during propagation. For mode with $\theta_{j,l}$, the recurrence exists only if $\theta_{j,l}$ satisfies

$$\lambda_{j,l}\theta_{j,l}/2 = 2\mu_{j,l}\pi, \tag{7}$$

where $\lambda_{j,l}$ is the effective wavelength, and $\mu_{j,l}$ is an integer. Note that $\lambda_{j,l}$ is also an integer considering the discreteness in the propagation direction. $\theta_{j,l}$ should thus be a rational multiple of π. Due to $\theta_{1,l} = -\theta_{2,l}$, the modes with $\theta_{1,l}$ and $\theta_{2,l}$ have the same effective wavelength that is denoted as λ_l. The Talbot distance is thus

$$z_T = \mathrm{LCM}(\lambda_0, \lambda_1, \lambda_2, ..., \lambda_{\mathcal{N}-1}), \tag{8}$$

in which LCM is the least common multiple.

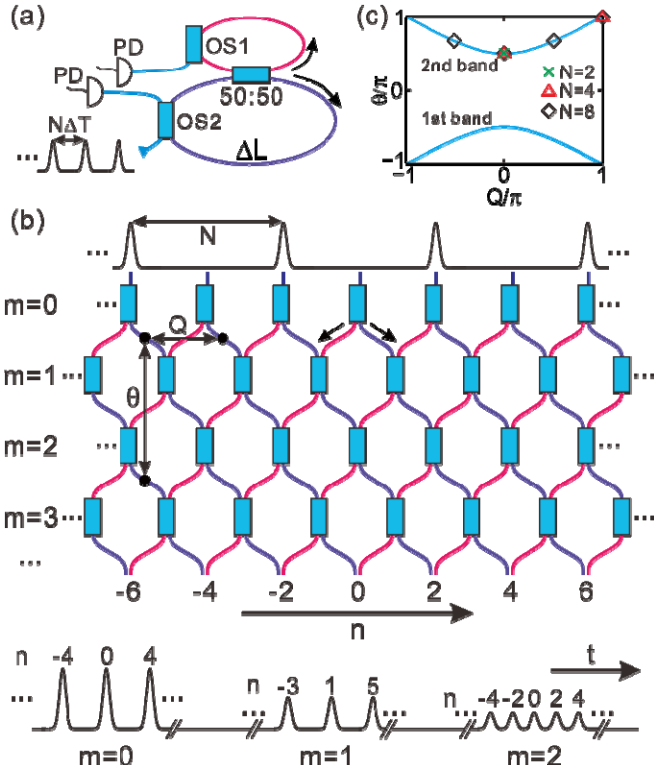

Fig. 1. (a) Schematic diagram of two coupled fiber loops. The short loop (marked in magenta) and long loop (marked in purple) are connected by a 50:50 directional coupler. OS1 and OS2 are 1 × 2 and 2 × 2 optical switches through which we can inject the initial pulse train to the long loop and couple out the pulse sequences from the loops. PD is photodiode. (b) Equivalent mesh lattice model for the two coupled fiber loops. The left path (marked in magenta) and right path (marked in purple) in the equivalent lattice correspond to short and long loops, respectively. The bottom insert is the stepwise evolution of pulse train in the long loop with the initial period being $N = 4$. (c) Band structure of the synthetic mesh lattice. The green crosses, red triangles and black diamonds represent the sets of Bloch modes at 2nd band for $N = 2$, 4, and 8, respectively.

Optics EXPRESS

We obtain the input periods allowing Talbot effect through enumeration method. Due to the existence of noises, the longest valid propagation distance is about M_L = 400 steps according to the experimental results [29–31]. From a practical point of view, the propagation distance that we consider only belongs to the set {1, 2, 3, ..., M_L}. Meanwhile, the initial period N should be no more than $2M_L$, otherwise the adjacent input pulses will exhibit ballistic spreading separately within M_L [26]. Considering the discreteness in the transverse direction, N is from {2, 4, 6, ..., $2M_L$}. Through enumerating all available input periods and propagation distances, the incident periods permitting Talbot revivals could be obtained. In detail, we choose the value of N at first and then calculate the set of $\theta_{2,l}$ according to Eq. (5). Note that $\theta_{1,l}$ is ignored due to $\theta_{1,l} = -\theta_{2,l}$. For mode with $\theta_{2,l}$, the recurrence occurs only if there exists a propagation distance m satisfying $m\theta_{2,l}/2 = 2\mu_{2,l}\pi$ among the set of m. The Talbot effect is supported only if all modes contained could exhibit revivals. As a result, the permitted input periods are N = 2, 4 and 8.

For N = 2, only the modes with Q_0 = 0 are contained. The corresponding propagation constant at 2nd band is $\theta_{2,0} = \pi/2$, as shown in Fig. 1(c). The mode with $\theta_{2,0}$ exhibits revival after 8 steps, which leads to the Talbot distance of z_T = 8. For N = 4, the modes with Q_0 = 0 and $Q_1 = \pi$ are contained. The corresponding propagation constants at 2nd band are $\theta_{2,0} = \pi/2$ and $\theta_{2,1} = \pi$, as illustrated in Fig. 1(c). The revival distances of the modes with $\theta_{2,0}$ and $\theta_{2,1}$ are 8 and 4, respectively. The Talbot distance is thus z_T = 8 which is the LCM of 4 and 8. For N = 8, the modes with Q_0 = 0, $Q_1 = \pi/2$, $Q_2 = \pi$ and $Q_3 = 3\pi/2$ are included therein. The propagation constants at 2nd band are $\theta_{2,0} = \pi/2$, $\theta_{2,1} = 2\pi/3$, $\theta_{2,2} = \pi$, and $\theta_{2,3} = 2\pi/3$ [Fig. 1(c)], and the corresponding revival distances are 8, 12, 4, and 12, respectively. The Talbot distance is z_T = 24 which is the LCM of 4, 8 and 12.

3. Results and discussion

3.1 Fundamental discrete temporal Talbot effect in synthetic mesh lattice

To verify the above theoretical analysis, we also perform numerical simulations for the pulse intensity evolutions by solving Eq. (1). As illustrated in Fig. 2(a) where we choose the incident period as N = 2, the input field recurs after the integer multiple of 8 steps, forming the typical pattern of Talbot carpet. The Talbot carpets with N = 4 and 8 are shown in Figs. 2(b) and 2(c), in which the revival distances are 8 and 24, respectively. The simulations can agree well with the above theoretical analysis. For other N, the Talbot effect cannot be supported, and we take the intensity evolution with N = 12 as an example to visualize the failure of Talbot self-imaging. As N = 12, the modes with $Q_1 = \pi/3$ should be contained. The corresponding propagation constant at 2nd band is $\theta_{2,1}$ = arccos(1/4) that is not rational multiple of π [32,33], and Eq. (7) will not be satisfied. The Talbot self-imaging is thus destroyed, as illustrated in Fig. 2(d) where the spread pattern becomes nonperiodic.

Similar to the continuous Talbot effect [3–5], the fractional Talbot images also appear during the process of discrete temporal Talbot effect. For N = 2, the fractional Talbot image exists at m = 4, as shown in Fig. 2(a). Note that the field at m = 4 has the same intensity distribution with the input one but accumulates a phase delay of π. For N = 4, the fractional Talbot images exist at m = 2, 4 and 6, as shown in Fig. 2(b). The intensity distributions at m = 2 and 6 have a period of 2 which is a half of N = 4. Accordingly, the repetition rate of the pulse train is doubled compared to the incident one. For N = 8, the period of intensity distribution at m = 12 is 2 which is a quarter of N = 8, as shown in Fig. 2(c). Accordingly, the repetition rate of pulse sequence is thus increased to 4 folds of the input one.

It should be mentioned that the fractional Talbot effect here could find applications in pulse repetition rate multiplication, passive amplification and temporal cloaking [8,15,16]. Specifically, as the pulse train propagates from the integer to the fractional Talbot distance or vice versa, as discussed above, the pulse repetition rate is scaled up (or down) by 2 or 4 times, making the intensity of each pulse being scaled down (or up), accordingly. So the processes

Optics EXPRESS

can realize the intensity redistribution of the pulse train, which can be applied to the pulse repetition rate multiplication from integer to fractional Talbot distance and pulse amplification vice versa. The mechanism of pulse amplification here does not rely on the active medium, which is termed as passive amplification, as firstly proposed in [16]. Note that from fractional to the integer Talbot distance, the pulse amplification is accompanied by the increase of time gap between adjacent pulses. And the enlarged time gap will be more beneficial to the realization of temporal cloaking within which an event could be hidden from being detected [15]. Compared to the continuous Talbot effect based on dispersive fiber system, the time gap here can be modified by changing the length difference of the two loops, which could be enlarged easily.

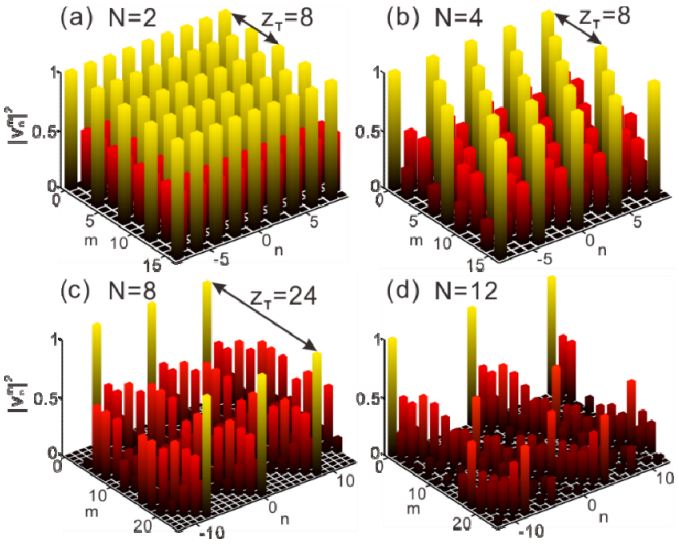

Fig. 2. (a)–(d) Pulse intensity evolutions in the long loop for N = 2, 4, 8 and 12, respectively.

3.2 The influence of coupling ratio on Talbot distance

We can tune the Talbot distance by controlling the splitting ratio of the coupler that connects two loops. We denote the splitting ratio as $\sin^2\alpha$:$\cos^2\alpha$ ($0 \le \alpha \le \pi/2$), and the band structure becomes

$$\cos\theta = \cos^2\alpha\cos Q - \sin^2\alpha. \tag{9}$$

We firstly consider the situation where $0 < \alpha < \pi/2$. For arbitrary choice of N and α, the modes with $Q_0 = 0$ are contained necessarily, and the corresponding propagation constant at 2nd band is $\theta_{2,0} = 2\alpha$. To ensure the revival of the mode with $\theta_{0,2}$, $\theta_{0,2}$ must satisfy Eq. (7), and thus α should be a rational multiple of π. Here we denote α as

$$\alpha = p\pi / q, \tag{10}$$

in which p and q are the relatively prime positive integers. Moreover, $q \ge 3$ and $q/4 \le p < q/2$ considering $\theta_{2,0} \in [\pi/2, \pi]$.

For N = 2, the corresponding propagation constant at 2nd band can only be $\theta_{2,0} = 2p\pi/q$. The Talbot distance is

$$z_T = 2q. \tag{11}$$

Considering $q \ge 3$ and $z_T \le M_L$, z_T should belong to {6, 8, 10, ..., M_L}. For N = 4, the propagation constants at 2nd band are $\theta_{2,0} = 2p\pi/q$ and $\theta_{2,1} = \pi$. The corresponding revival

Optics EXPRESS

distances are $2q$ and 4, respectively. The Talbot distance is the LCM of 4 and $2q$, which can be expressed as

$$z_T = \begin{cases} 4q & (p \text{ is odd}), \\ 2q & (p \text{ is even}). \end{cases} \tag{12}$$

Due to $q \geq 3$ and $z_T \leq M_L$, z_T should be from $\{8, 12, 16, ..., M_L\}$. We show the Talbot distance varying with α and N in Fig. 3(a). For $N = 2$, the Talbot distance becomes 12 (18) as q is 6 (9). For $N = 4$, we can tune the Talbot distance to 12 by choosing q as 6. The Talbot carpets shown in Figs. 3(b)–3(d) coincide well with the above theoretical analysis. For $N > 4$, we also study the Talbot revivals through enumeration method. To guarantee that the mode with $\theta_{2,0} = 2p\pi/q$ could revive within M_L, q should be no more than $M_L/2$. Considering $3 \leq q \leq M_L/2$ and $q/4 \leq p < q/2$, α should be from a finite set, which enables us to enumerate the values of α for the purpose of finding the allowed ones. It turns out that the Talbot revivals occur only if $\alpha = \pi/4$ and $N = 8$. Because $\alpha = \pi/4$ corresponds to a coupling ratio of 50:50, this case has been discussed in Sec. 2.

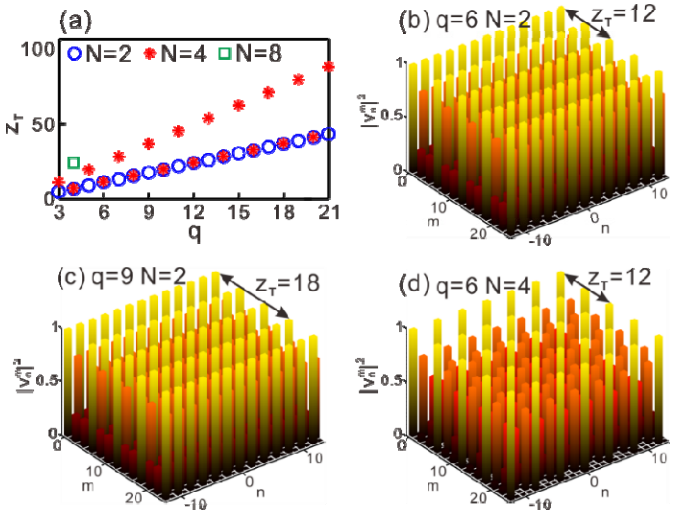

Fig. 3. (a) Talbot distance z_T versus q. (b) (c) Talbot carpets for $q = 6$ and 9 as $N = 2$. (d) Talbot carpet for $q = 6$ as $N = 4$.

Optics EXPRESS

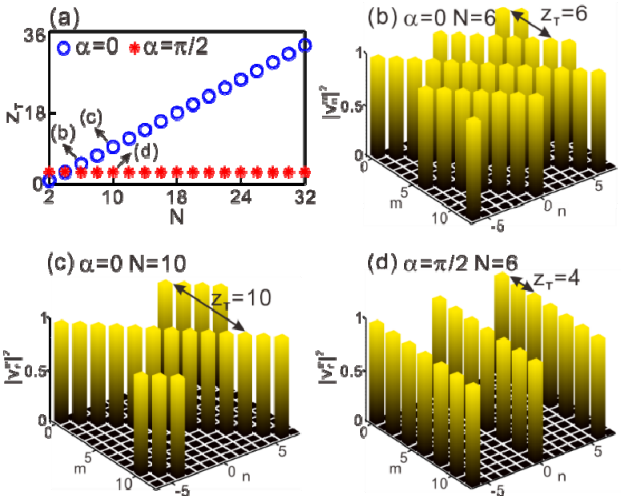

Fig. 4. (a) The variation of Talbot distance z_T versus the input period N as $\alpha = 0$ and $\pi/2$. (b) (c) Talbot carpets with $N = 6$ and 10 as $\alpha = 0$. (d) Talbot carpet for $N = 6$ as $\alpha = \pi/2$.

We now focus on the Talbot effects for $\alpha = 0$ and $\pi/2$. For $\alpha = 0$, corresponding to a splitting ratio of 0:1, the band structure reads

$$\theta = \pm Q. \tag{13}$$

For arbitrary choice of $\mathcal{N}$, the corresponding propagation constants at 2nd band should be in the form of $\theta_{2,l} = 2\pi l/N$. The Talbot distance is thus $z_T = N$. We illustrate the Talbot distance z_T varying with the input period N in Fig. 4(a). Due to $z_T \le M_L$, z_T belongs to $\{2, 4, 6, ..., M_L\}$. We show the Talbot carpets of $N = 6$ and $N = 10$ in Figs. 4(b) and 4(c) where the incident fields exhibit recurrence after 6 and 10 steps, respectively. For $\alpha = \pi/2$, corresponding to a coupling ratio of 1:0, the band structure is

$$\theta = \pi. \tag{14}$$

For arbitrary choice of N, all modes have a propagation constant of $\theta = \pi$. The Talbot distance is $z_T = 4$ which is independent of the input period N, as shown in Fig. 4(a). The Talbot carpet with $N = 6$ is shown in Fig. 4(d) where the input field exhibits revivals after every 4 steps. In the above two cases, the repetition rate of pulse train shows no change during propagation because no coupling exists for $\alpha = 0$ and the coupler acts as a circulator for $\alpha = \pi/2$.

3.3 The influence of initial Bloch momentum on Talbot distance

We now impose a stepwise phase modulation on the incident pulse sequence, and the interval between phase shifts imposed on adjacent pulses is denoted as ϕ_0. Accordingly, the incident field acquires an initial Bloch momentum ϕ_0 in the synthetic mesh lattice, as shown in Fig. 5(a). The Bloch momenta should thus be in the form of

$$Q_l = 2\pi l / \mathcal{N} + \phi_0. \tag{15}$$

For $N = 2$, the Bloch momenta is $Q_0 = \phi_0$, and the corresponding propagation constant at 2nd band reads

$$\theta_{2,0} = \arccos[(\cos\phi_0 - 1)/2]. \tag{16}$$

The Talbot effect exists only if $\theta_{2,0}$ satisfies Eq. (7). $\theta_{2,0}$ is in the form of

$$\theta_{2,0} = a\pi / b, \tag{17}$$

Optics EXPRESS

where a and b are the relative prime positive integers. Moreover, $b \geq 1$ and $b/2 \leq a \leq b$ due to $\theta_{2,0} \in [\pi/2, \pi]$. The Talbot distance is

$$z_T = \begin{cases} 4b & (a \text{ is odd}), \\ 2b & (a \text{ is even}), \end{cases} \tag{18}$$

and $z_T \in \{4, 6, 8, ..., M_L\}$. The corresponding initial Bloch momenta ϕ_0 is derived from Eq. (16), which can be expressed as

$$\phi_0 = \arccos(2\cos\theta_{0,2} + 1). \tag{19}$$

Considering that the band structure is symmetric in Q axis, ϕ_0 and $-\phi_0$ have the same impacts on $\theta_{2,0}$, and thus the corresponding Talbot distances are same. We illustrate the Talbot distance z_T varying with $|\phi_0|$ in Fig. 5(b). The Talbot carpet with $\phi_0 = 0.71\pi$ is shown in Fig. 5(c) where the Talbot distance is tuned to $z_T = 10$.

For $N = 4$, the modes with $Q_0 = \phi_0$ and $Q_1 = \pi + \phi_0$ are included. The propagation constants at 2nd band read

$$\begin{cases} \theta_{2,0} = \arccos[(\cos\phi_0 - 1)/2], \\ \theta_{2,1} = \arccos[(-\cos\phi_0 - 1)/2]. \end{cases} \tag{20}$$

We find the allowed values of ϕ_0 through the enumeration method. To support the Talbot effect, $\theta_{2,0}$ and $\theta_{2,1}$ are both in the form of $a\pi/b$. Due to $\lambda_0, \lambda_1 \leq M_L$, b is no more than $M_L/2$. Considering $1 \leq b \leq M_L/2$ and $b/2 \leq a \leq b$, $\theta_{2,0}$ and $\theta_{2,1}$ should belong to a finite set, which enables the enumeration method. The Talbot revivals are supported only when $|\phi_0|$ is $\pi/2$ or π, and the corresponding Talbot distances are 6 and 8, respectively. We illustrate the Talbot carpet with $\phi_0 = \pi/2$ in Fig. 5(d) where the Talbot distance is tuned to 6. For $N = 8$, we also use the enumeration method to find the available values of ϕ_0. The Talbot recurrence occurs as $|\phi_0|$ is chosen from $\{\pi/2, \pi\}$, but the Talbot distance is not influenced.

Optics EXPRESS

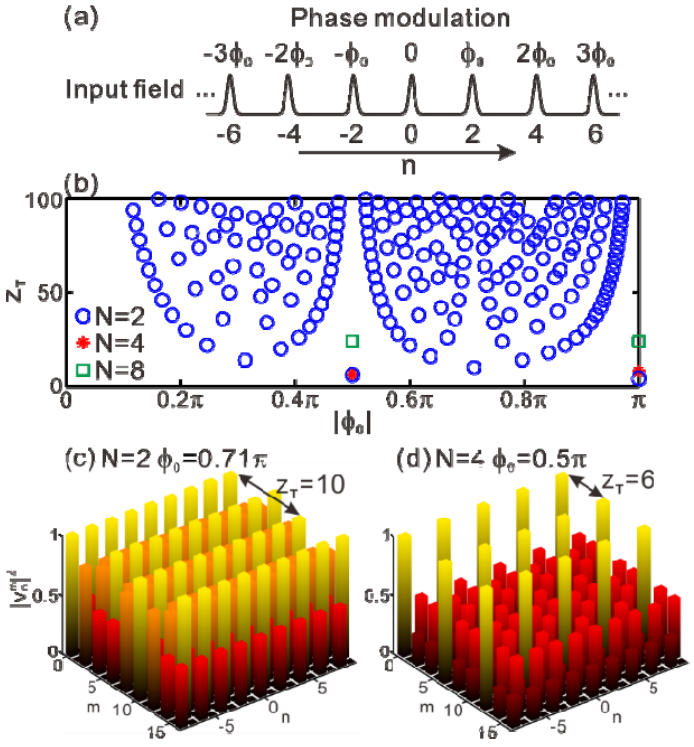

Fig. 5. (a) Schematic of the incident field under stepwise phase modulation. (b) Talbot distance z_T versus initial momentum ϕ_0. (c) Talbot carpet with $N = 2$ and $\phi_0 = 0.71\pi$. (d) Talbot carpet with $N = 4$ and $\phi_0 = 0.5\pi$.

3.4 Talbot effect with fractional incident period

In the spatial lattice, the incident beams can only be coupled into the input ports, otherwise they will decay exponentially. The period number of periodic incident field must thus be an integer. Nevertheless, the pulse train with arbitrary period could be injected into the two coupled fiber loops. Accordingly, the input period could be an arbitrary positive number in synthetic mesh lattice. We firstly consider the situation where N is rational. The incident period is represented as

$$N = 2K / L, \tag{21}$$

in which K and L are the relative prime positive integers.

From the aspect of the coupled loops, the incident pulse sequence could be treated as a combination of several sparse sequences that evolve in coupled loops independently. From the aspect of synthetic mesh lattice, the incident field with period $2K/L$ is decomposed to certain identical fields with period $2K$. Moreover, these individual fields are uniformly spaced in the transverse direction and injected to separated lattices, as shown in Fig. 6(a). The coupled loops is thus multiplexed in the time domain, which leads to that several independent synthetic mesh lattices exist at the same time. In an individual lattice, the incident period allowing Talbot effect is not affected, the Talbot distance z_T also shows no change. Interestingly, the allowed input periods could be extended vastly and denoted as $N = 2K_T/L$, where $K_T = 1$, 2, and 4. We illustrate the Talbot distance varying with K and L in Fig. 6(b). The Talbot carpets of $N = 2/3$, 4/3 and 8/3 shown in Figs. 6(c)–6(e) agree well with the above theoretical analysis. As the incident period N is irrational, the Talbot effect will not be supported because the input field cannot be decomposed to several fields with period being 2, 4 or 8.

Optics EXPRESS

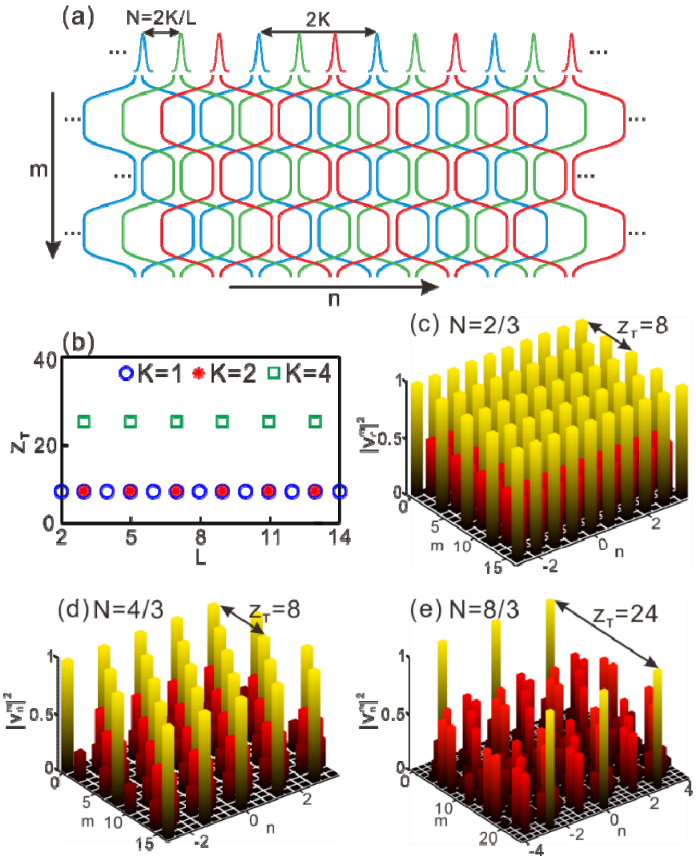

Fig. 6. (a) Schematic of the separated synthetic mesh lattices uniformly spaced in the transverse direction. The incident field with period $N = 2K/L$ is decomposed to several identical fields with period $2K$ distinguished by color which evolve in the lattices in the same color independently. (b) Talbot distance z_T versus K and L. (c)-(e) Talbot carpets of $N = 2/3$, 4/3 and 8/3, respectively.

Since bandwidth is an essential issue in the context of optical pulse propagation, now we compare the dispersion effects of discrete temporal Talbot effect with conventional continuous temporal Talbot effect in dispersive fibers. The continuous temporal Talbot effect depends on the second-order dispersion, the bandwidth of which is limited by the higher-order dispersions of fiber [17]. Here the discrete temporal Talbot effect is based on the diffraction in the periodic time lattice created by two coupled fiber loops. The bandwidth is limited by both the second- and high-order dispersions, such that wide pulses should be chosen. However, due to the short length for the fiber loop that is about several meters, the pulse width can still be chosen as short as picosecond to get rid of dispersions [34]. Therefore, the discrete temporal Talbot effect can still manifest comparable bandwidth with the continuous case. Compared to the continuous Talbot effect in fiber, we can further increase the bandwidth by reducing the loop length or using the dispersion compensation components [35]. For practical applications, broad bandwidth will be benefit to the realization of discrete Talbot effect for even shorter pulses.

In terms of the applications, the features of period dependence and Talbot distance tunability of discrete temporal Talbot effect will benefit the following application aspects. For the pulse amplification and repetition rate multiplication, different choice of the incident period can be used to select different amplification factors. For temporal cloaking, different incident period can also benefit the precise control of time cloaking window. All the

Optics EXPRESS

processes could be flexibly tuned by the Talbot distances via changing the splitting ratio of coupler or the length of fiber loops.

Finally, the discrete temporal Talbot effect is also affected by the length of fiber loops and the loop propagation loss. The Talbot effect requires sufficient long fiber loop with more pulses to mimic the periodic input condition, while the presence of dispersions requires short loop to increase the bandwidth. The tradeoff can be balanced by choosing a relative long fiber loop to accommodate more pulse while compensating the dispersions. For the propagation loss, although it has no influence on the conditions of Talbot effect, we can utilize optical amplifier to compensate the loss, such that the discrete Talbot effect could be more readily to observe. Moreover, the two coupled loops might be transferred into the integrated waveguides with the geometric structure and dispersion property being carefully designed.

4. Conclusion

In conclusion, we have investigated the discrete temporal Talbot effect in the synthetic mesh lattice based on two coupled fiber loops. The Talbot revivals occur only if the normalized incident period are N = 2, 4 and 8, and the corresponding Talbot distances are 8, 8 and 24, respectively. Due to the existence of fractional Talbot effect, the repetition rate of pulse train can be increased at fractional multiple of Talbot distance and become 4 multiples of the input one at most. By controlling the splitting ratio of the coupler which is related to the band structure, the Talbot distance can be flexibly tuned, and the set of available Talbot distances becomes {2, 4, 6, ..., M_L} with M_L being the longest valid propagation distance. By imposing stepwise phase modulation on the incident pulse sequence, the Talbot distance is tunable since the initial momentum of the incident field varies. Through the time-multiplexing of coupled loops, the incident periods allowing Talbot effect can be extended to 2/L, 4/L and 8/L with L being an integer. The study may find great applications in temporal cloaking, passive amplification, and pulse repetition rate multiplication.

Funding

Program 973 (2014CB921301); National Natural Science Foundation of China (NSFC) (11674117).

References and links

1. H. F. Talbot, “Facts relating to optical science,” Philos. Mag. **9**(56), 401–407 (1836).
2. L. Rayleigh, “On copying diffraction-gratings, and on some phenomena connected therewith,” Philos. Mag. **11**(67), 196–205 (1881).
3. J. T. Winthrop and C. R. Worthington, “Theory of Fresnel images. I. plane periodic objects in monochromatic light,” J. Opt. Soc. Am. **55**(4), 373–381 (1965).
4. K. Patorski, “Self-imaging and its applications,” in *Progress in Optics XXVII*, E. Wolf, ed. (Elsevier, 1989).
5. M. V. Berry and S. Klein, “Integer, fractional and fractal Talbot effects,” J. Mod. Opt. **43**(10), 2139–2164 (1996).
6. T. Jannson and J. Jannson, “Temporal self-imaging effect in single-mode fibers,” J. Opt. Soc. Am. **71**(11), 1373–1376 (1981).
7. B. H. Kolner, “Space-time duality and the theory of temporal imaging,” IEEE J. Quantum Electron. **30**(8), 1951–1963 (1994).
8. J. Azaña and M. A. Muriel, “Technique for multiplying the repetition rates of periodic trains of pulses by means of a temporal self-imaging effect in chirped fiber gratings,” Opt. Lett. **24**(23), 1672–1674 (1999).
9. J. Azaña and M. A. Muriel, “Temporal Talbot effect in fiber gratings and its applications,” Appl. Opt. **38**(32), 6700–6704 (1999).
10. S. Longhi, M. Marano, P. Laporta, O. Svelto, M. Belmonte, B. Agogliati, L. Arcangeli, V. Pruneri, M. N. Zervas, and M. Ibsen, “40-GHz pulse-train generation at 1.5 μm with a chirped fiber grating as a frequency multiplier,” Opt. Lett. **25**(19), 1481–1483 (2000).
11. J. Azaña and M. A. Muriel, “Temporal self-imaging effects: theory and application for multiplying pulse repetition rates,” IEEE J. Sel. Top. Quantum Electron. **7**(4), 728–744 (2001).
12. D. Pudo, M. Depa, and L. R. Chen, “Single and multiwavelength all-optical clock recovery in single-mode fiber using the temporal Talbot effect,” J. Lightwave Technol. **25**(10), 1729–1733 (2007).
13. J. M. Lukens, D. E. Leaird, and A. M. Weiner, “A temporal cloak at telecommunication data rate,” Nature **498**(7453), 205–208 (2013).

Optics EXPRESS

14. J. M. Lukens, A. J. Metcalf, D. E. Leaird, and A. M. Weiner, "Temporal cloaking for data suppression and retrieval," Optica **1**(6), 372–375 (2014).
15. B. Li, X. Wang, J. Kang, Y. Wei, and K. K.-Y. Wong, "Extended time cloak based on inverse temporal Talbot effect," in *Conference on Lasers and Electro-Optics*, OSA Technical Digest (Optical Society of America, 2017), paper SF2L.2.
16. R. Maram, J. Van Howe, M. Li, and J. Azaña, "Noiseless intensity amplification of repetitive signals by coherent addition using the temporal Talbot effect," Nat. Commun. **5**(1), 5163 (2014).
17. J. Fatome, S. Pitois, and G. Millot, "Influence of third-order dispersion on the temporal Talbot effect," Opt. Commun. **234**(1), 29–34 (2004).
18. R. Iwanow, D. A. May-Arrioja, D. N. Christodoulides, G. I. Stegeman, Y. Min, and W. Sohler, "Discrete Talbot effect in waveguide arrays," Phys. Rev. Lett. **95**(5), 053902 (2005).
19. Y. Wang, K. Zhou, X. Zhang, K. Yang, Y. Wang, Y. Song, and S. Liu, "Discrete plasmonic Talbot effect in subwavelength metal waveguide arrays," Opt. Lett. **35**(5), 685–687 (2010).
20. F. Wang, C. Qin, B. Wang, H. Long, K. Wang, and P. Lu, "Rabi oscillations of plasmonic supermodes in graphene multilayer arrays," IEEE J. Sel. Top. Quantum Electron. **23**(1), 4600105 (2017).
21. H. Ramezani, D. N. Christodoulides, V. Kovanis, I. Vitebskiy, and T. Kottos, "PT-symmetric Talbot effects," Phys. Rev. Lett. **109**(3), 033902 (2012).
22. Y. Fan, B. Wang, K. Wang, H. Long, and P. Lu, "Talbot effect in weakly coupled monolayer graphene sheet arrays," Opt. Lett. **39**(12), 3371–3373 (2014).
23. K. Li, F. Xia, M. Wang, P. Sun, T. Liu, W. Hu, W. Kong, M. Yun, and L. Dong, "Discrete Talbot effect in dielectric graphene plasmonic waveguide arrays," Carbon **118**, 192–199 (2017).
24. F. Wang, S. Ke, C. Qin, B. Wang, H. Long, K. Wang, and P. Lu, "Topological interface modes in graphene multilayer arrays," Opt. Laser Technol. **103**, 272–278 (2018).
25. S. Ke, D. Zhao, Q. Liu, S. Wu, B. Wang, and P. Lu, "Optical imaginary directional couplers," J. Lightwave Technol. **36**(12), 2510–2516 (2018).
26. A. Regensburger, C. Bersch, B. Hinrichs, G. Onishchukov, A. Schreiber, C. Silberhorn, and U. Peschel, "Photon propagation in a discrete fiber network: an interplay of coherence and losses," Phys. Rev. Lett. **107**(23), 233902 (2011).
27. A. Regensburger, C. Bersch, M. A. Miri, G. Onishchukov, D. N. Christodoulides, and U. Peschel, "Parity-time synthetic photonic lattices," Nature **488**(7410), 167–171 (2012).
28. C. Qin, F. Zhou, Y. Peng, D. Sounas, X. Zhu, B. Wang, J. Dong, X. Zhang, A. Alù, and P. Lu, "Spectrum control through discrete frequency diffraction in the presence of photonic gauge potentials," Phys. Rev. Lett. **120**(13), 133901 (2018).
29. I. D. Vatnik, A. Tikan, G. Onishchukov, D. V. Churkin, and A. A. Sukhorukov, "Anderson localization in synthetic photonic lattices," Sci. Rep. **7**(1), 4301 (2017).
30. M. Wimmer, H. M. Price, I. Carusotto, and U. Peschel, "Experimental measurement of the Berry curvature from anomalous transport," Nat. Phys. **13**(6), 545–550 (2017).
31. M. Wimmer, M. A. Miri, D. Christodoulides, and U. Peschel, "Observation of Bloch oscillations in complex PT-symmetric photonic lattices," Sci. Rep. **5**(1), 17760 (2015).
32. J. Varona, "Rational values of the arccosine function," Open Math. **4**(2), 319–322 (2006).
33. M. Aigner, G. M. Ziegler, and A. Quarteroni, *Proofs from the Book,* 4nd ed. (Springer, 2010).
34. B. Ainslie and C. Day, "A review of single-mode fibers with modified dispersion characteristics," J. Lightwave Technol. **4**(8), 967–979 (1986).
35. L. Grüner-Nielsen, S. N. Knudsen, B. Edvold, T. Veng, D. Magnussen, C. C. Larsen, and H. Damsgaard, "Dispersion compensating fibers," Opt. Fiber Technol. **6**(2), 164–180 (2000).